Langmuir

Article

pubs.acs.org/Langmuir

Evaporation of Drops on Two Parallel Fibers: Influence of the Liquid Morphology and Fiber Elasticity

Camille Duprat,[†,‡] Alison D. Bick,[†] Patrick B. Warren,[§] and Howard A. Stone*[,†]

[†]Department of Mechanical and Aerospace Engineering, Princeton University, Princeton, New Jersey 08544, United States

[§]Unilever Research and Development Port Sunlight, Quarry Road East, Bebington, Wirral CH63 3JW, United Kingdom

ABSTRACT: We investigate experimentally the evaporation of liquid accumulated on a pair of parallel fibers, rigid or flexible. The liquid wetting the fibers can adopt two distinct morphologies: a compact drop shape, whose evaporation dynamics is similar to that of an isolated aerosol droplet, or a long liquid column of constant cross-section, whose evaporation dynamics depends upon the aspect ratio of the column. We thus find that the evaporation rate is constant for drops, while it increases strongly for columns as the interfiber distance decreases, and we propose a model to explain this behavior. When the fibers are flexible, the transition from drops to columns can be induced by the deformation of the fibers because of the capillary forces applied by the drop. Thus, we find that the evaporation rate increases with increasing flexibility. Furthermore, complex morphology transitions occur upon drying, which results in spreading of the drop as it evaporates.

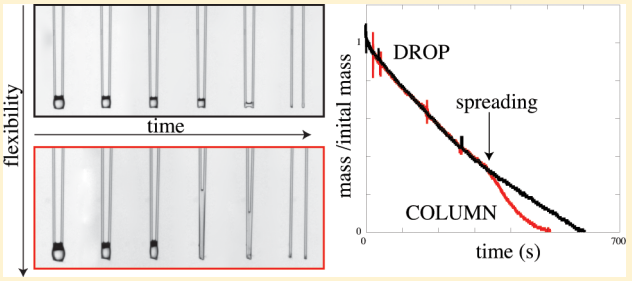

INTRODUCTION

The evaporation of a sessile macroscopic droplet is a familiar phenomenon that enters many industrial processes, such as spray cooling, particle deposition, and heat exchange. Starting from the seemingly simple case of an aerosol droplet evaporating in a quiescent atmosphere,[1] the dynamics of evaporation of a drop resting on a surface has been studied extensively, both experimentally and theoretically.[2,3] Most studies considered the effect of the wetting properties of the substrate, i.e., the influence of the contact angle on the dynamics, from hydrophilic to super-hydrophobic or textured surfaces.[4−7] However, the effect of the mechanical properties of the substrate (i.e., its elasticity) has been addressed only recently, because of the increased use of soft viscoelastic gels. When a drop is deposited on a soft solid, the capillary forces at the contact line and the Laplace pressure within the drop can deform the surface.[8−12] The deformation at the triple-phase contact line affects the receding contact angle and can result in pinning of the contact line.[13−15] Upon drying, the drop will thus maintain a constant contact radius; consequently, droplets evaporate faster on softer surfaces.

When the substrate is not a flat surface but rather a structured porous structure, the evaporation dynamics of isolated droplets becomes increasingly complicated. In particular, significant attention has been given to transpiration from fibrous media. For example, the drying dynamics of collected aerosol drops from a fibrous filter, present in many industrial settings, does not follow the laws estimated by the evaporation of spherical particles suspended in quiescent air.[16] However, only the global evaporation from the material was considered, and the relation to the local behavior of single drops remains unexplored. Furthermore, the presence of liquid/air interfaces induces capillary forces that can deform locally the fibers, thus affecting the liquid distribution.[17,18] This elastocapillary effect causes the shrinkage of a fibrous membrane upon drying because of the collapse of adjacent fibers[19] or can be used to induce self-assembly of micro- or nanopillars.[20−22]

To understand the drying dynamics of a fiber array, we start by looking at the evaporation of a single isolated drop. We choose a model system consisting of two parallel fibers and investigate both rigid fibers and flexible fibers; i.e., we quantify the effect of elasticity on the evaporation process by allowing bending of the pair of fibers.

RIGID FIBERS

A liquid deposited on two parallel rigid fibers can adopt different morphologies, either a compact hemispherical drop or a long liquid column of uniform cross-section.[23−26] We focus here on perfectly wetting liquids, i.e., with an equilibrium contact angle $\theta_e = 0$. Previously, we obtained a morphology diagram[27] as a function of the drop volume V and the interfiber distance $2d$, renormalized by the fiber radius r (Figure 1a). Columns only exist for $d/r < \sqrt{2}$, while drops prevail for $d/r > \sqrt{2}$. For large volumes $V/r^3 > 500$, there is a range of separation distances $0.57 < d/r < \sqrt{2}$ for which drops are also more energetically favorable. However, in that region, columns are metastable and both column and drop states are observed.

Received: March 27, 2013
Revised: May 17, 2013

   dx.doi.org/10.1021/la4011532 | *Langmuir* XXXX, XXX, XXX−XXX

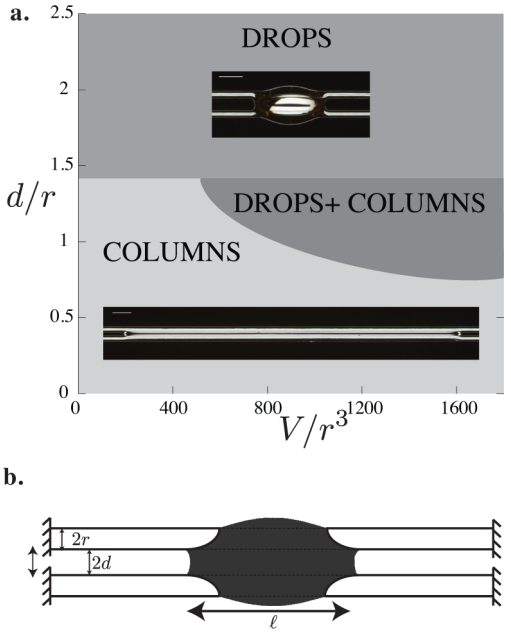

Figure 1. (a) Morphology diagram of a volume V of liquid deposited on two rigid parallel fibers of radius r separated by a distance d. Scale bars = 1 mm. (b) Experimental setup: a wetting drop (silicone oil) is deposited on two parallel fibers (nylon or glass).

Experimental Setup. We consider the ideal case of isothermal diffusion-dominated evaporation of perfectly wetting liquids on a pair of rigid parallel fibers of various radii, as sketched in Figure 1b. The distance between the fibers $2d$ is adjusted using two microcontrolled stages. The drop volume V is typically 2−5 μL; therefore, the drop size is typically $R \simeq 0.5$ mm. We used two low-viscosity perfectly wetting silicone oils, one with density $\rho = 760$ kg/m^3, surface tension $\gamma = 15.9$ mN/m, and kinematic viscosity $\nu = 0.65$ mm^2/s (SO65) and the other one with density $\rho = 818$ kg/m^3, surface tension $\gamma = 16.9$ mN/m, and kinematic viscosity $\nu = 1$ mm^2/s (SO1). The Bond number $Bo = \rho g R^2/\gamma$ that compares surface tension and gravitational forces is of the order 0.1; surface tension effects will thus dominate over gravity effects. These oils have different diffusivities in air, which leads to an order of magnitude difference in the evaporation rate. The density of oil in air is ρ_S. We suppose that, at the interface, we are at thermodynamic equilibrium and $\rho_S = \rho_{sat}$ the density at saturation and that, far from the liquid, the density tends toward $\rho_S \to \rho_\infty = 0$. We assume that evaporation is solely driven by diffusion. The diffusive process is modeled by Fick's law, while we have to solve the Laplace equation to obtain the concentration profile. However, we can deduce the oil diffusivities and saturation density by measuring the evolution of mass with time during the evaporation from a fixed surface (i.e., a Petri dish of radius R_p) using precision scales. We then deduce the rate χ at which the liquid evaporates and find $\chi = (3 \pm 0.1) \times 10^{-4}$ g/s (SO65) and $\chi = (5 \pm 1) \times 10^{-5}$ g/s (SO1). For a disk of radius R_p, if evaporation is diffusion-dominated, the mass flux is given by $\chi = 8 D_m \rho_{sat} R_p$. We thus obtain $D_m \rho_{sat} = (1.47 \pm 0.05) \times 10^{-6}$ kg m^{-1} s^{-1} (SO65) and $D_m \rho_{sat} = (2.4 \pm 0.5) \times 10^{-7}$ kg m^{-1} s^{-1} (SO1) and can further determine an evaporation parameter $D = D_m(\rho_{sat}/\rho)$ that has the dimensions of a diffusion coefficient. We find $D = (19.3 \pm 0.7) \times 10^{-10}$ m^2/s (SO65) and $D = (2.9 \pm 0.6) \times 10^{-10}$ m^2/s (SO1), in agreement with the values reported in the literature.[2]

Evaporation of a Drop on a Single Fiber. We first perform a control experiment by monitoring the evaporation of a drop on a single fiber. We measure the evolution of the length of the drop $l(t)$, and we denote t_f the time at which all of the liquid has disappeared (Figure 2). Because the liquid is perfectly wetting the fibers ($\theta_e = 0$), the drop adopts a barrel unduloid shape throughout evaporation.[28,29] For a given fiber radius, when the length is plotted as a function of the rescaled time $D(t_f - t)$, the data for the two oils collapse on a single curve, which indicates that the evaporation process is indeed diffusion-dominated.

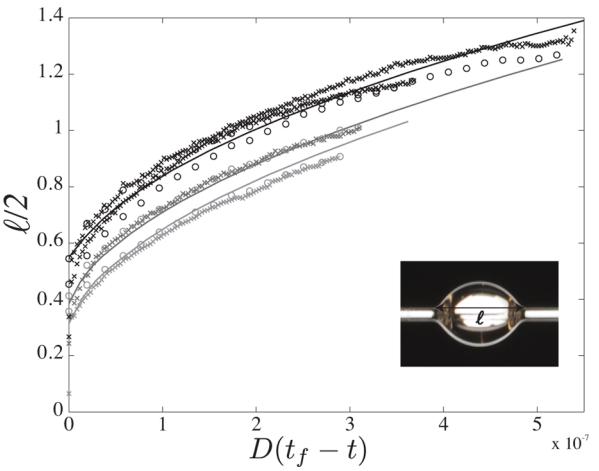

Figure 2. Evaporation of the length $l/2$ (mm) of a drop on a single fiber for two different oils as a function of $D(t_f - t)$ (m^2): for SO65, $\nu = 0.65$ mm^2/s, $\rho = 760$ kg/m^3, and $D = 19 \times 10^{-10}$ m^2/s (○) and for S01, $\nu = 1$ mm^2/s, $\rho = 818$ kg/m^3, and $D = 3 \times 10^{-10}$ m^2/s (×) and three fiber radii: $2r = 0.2$ mm (light gray), $2r = 0.245$ mm (gray), and $2r = 0.35$ mm (black). The model described in the text and Appendix is given by the solid lines.

A mass balance can be written

$$\rho \frac{dV}{dt} = \phi A \tag{1}$$

where A is the surface area and ϕ is the mass flux per unit area. For a spherical droplet of radius R, the concentration profile is obtained by solving the Laplace equation in spherical coordinates, which, using Fick's law for the diffusive process,[1] gives the diffusive flux $j_0 = \phi/\rho = -D/R$. The solution of eq 1 is thus $R(t) = (2D(t_f - t))^{1/2}$, which is the classical so-called "D^2" law.[2] In the case of a drop on a fiber, the drop slightly departs from the spherical shape and adopts an unduloid barrel shape of length l. We assume that the flux remains radial, with a diffusive length $l/2$, i.e., $j_0 = -D/(l/2)$, and the shape of the drop, i.e., length l and surface area A as a function of the volume V and the fiber radius r, can be found analytically[30] (see the Appendix). For a fixed volume, as we increase the fiber radius, the drop departs further from a sphere and flattens toward a more cylindrical shape, resulting in an increase in length l. During evaporation, as the volume is reduced, the drop adopts successive barrel shapes of decreasing length (Figure 2). We can solve eq 1 numerically to obtain $l(t)$. We find a good agreement with the experiments, indicating that the assumption of a radial flux with a typical diffusive length $l/2$ is a good first approximation (Figure 2).

Evaporation from Two Fibers. We can now study the evaporation of liquid from a pair of rigid parallel fibers with

dx.doi.org/10.1021/la4011532 | Langmuir XXXX, XXX, XXX−XXX

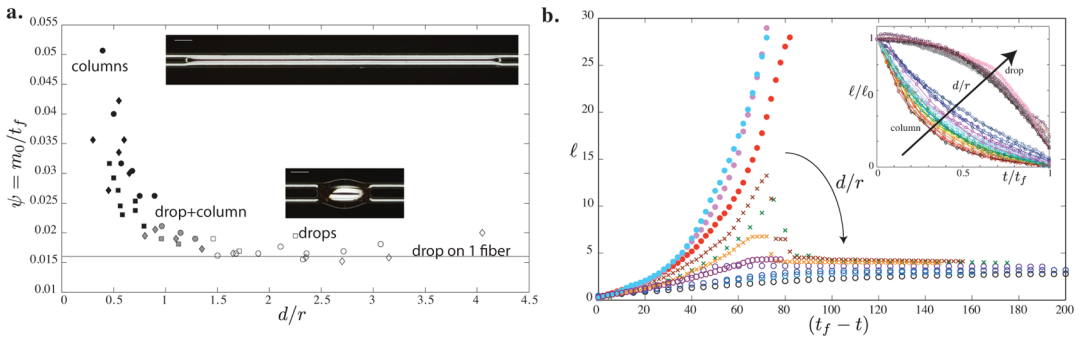

Figure 3. (a) Average evaporation rate ψ (mg/s) as a function of the distance between the fibers d/r for different fiber radii: $2r$ = 0.2 mm (squares), $2r$ = 0.245 mm (circles), and $2r$ = 0.35 mm (diamonds) and silicone oil SO65. The liquid adopts different morphologies, from drops (open symbols) to columns (black symbols). There is a range of d/r where both states coexist (gray symbols). Similar results are obtained for SO1 (not shown) with an average evaporation rate of the order 10^{-3} mg/s. (b) Evolution of the wetted length l (mm) on two parallel fibers of radius 0.2 mm as the liquid (SO1) evaporates as a function of time $(t_f - t)$ (s). The liquid is in either a drop state (open circles) or a column state (closed circles), or it exhibits both states during evaporation (crosses). (Inset) Rescaled length l/l_0 as a function of the rescaled time t/t_f for various distances between the fibers, fiber radii, and initial volumes.

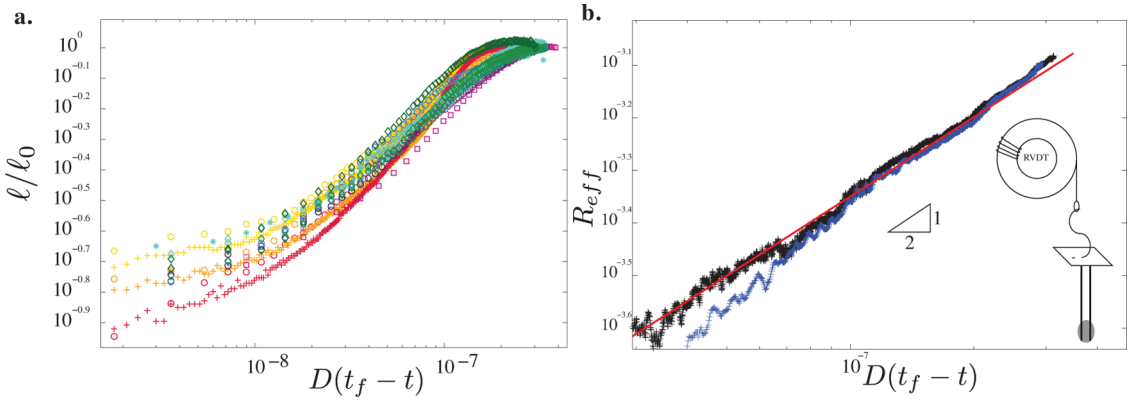

Figure 4. Evaporation in the drop morphology ($d/r > \sqrt{2}$). (a) Evolution of the rescaled length l/l_0 as a function of rescaled time $D(t_f - t)$ (m^2) for $2r$ = 0.2 mm (○, +), $2r$ = 0.245 mm (◇, ×), and $2r$ = 0.35 mm (□, ∗) for SO65 and S01, respectively, and varying $1.5 < d/r < 4$. (b) Evolution of the effective radius $R_{eff} = (3V/4\pi)^{1/3}$ (mm) with time $D(t_f - t)$ (m^2) for $2r$ = 0.29 mm, d/r = 2.6, and silicone oil SO1 (black) and SO65 (blue) with $D = 3 \times 10^{-10}$ and 19×10^{-10} m^2/s, respectively. The line is eq 2. (Inset) Schematic of the setup used to measure the drop mass with time.

radii r and spacing d. We first measure the average evaporation rate ψ, defined as the ratio of the initial mass m_0 to the evaporation time t_f, as we vary d/r for a given liquid and different fiber radii (Figure 3a). We observe that, for $d/r > \sqrt{2}$, as the liquid adopts a drop shape, the evaporation rate is constant and equal to that of a drop on a single fiber. We can estimate the order of magnitude of this average evaporation rate with the rate obtained for an isolated aerosol droplet: for a drop of initial radius is R_0, the total evaporation time $t_f = {R_0}^2/(2D)$ and $\psi = m_0/t_f = (8/3)\rho\pi R_0 D$. For a microliter droplet, $R_0 \sim 0.5$ mm, and $\psi \sim 2 \times 10^{-2}$ mg/s (SO65) or $\psi \sim 3.63 \times 10^{-3}$ mg/s (SO1), in good agreement with the experimental values of 1.6×10^{-2} mg/s for SO65 and 3×10^{-3} mg/s for SO1. However, as the liquid adopts a column shape, there is a sharp increase in the evaporation rate as d/r decreases. This increase can be partially understood by the increase in surface area as the liquid spreads into a column. We will now study the drying kinetics of both drops and columns to quantify and understand these observations.

We measure the evolution of the wetted length l with time $t_f - t$ as shown in Figure 3b. Dependent upon the interfiber distance, we observe long columns with fast evaporation, drops with slow evaporation, or cases where both states are reached during evaporation. The latter case is observed for distances $0.57 < d/r < \sqrt{2}$. We start with a large volume of liquid ($V/r^3 > 700$) for which the drop shape is the most stable configuration (see Figure 1a). As the liquid evaporates and the volume is reduced (i.e., traveling horizontally in the morphology diagram of Figure 1a), the column becomes more favorable and the liquid spreads and then evaporates. These situations are reported in Figure 3b (crosses): the length l first follows the drop behavior and then switches to the column behavior.

To compare the dynamics, we rescale the data with the initial length l_0 and the evaporation time t_f (inset in Figure 3b). There are two clear trends for drops and columns. All of the data for the drops collapse on a single curve, while the data for columns exhibit a clear dependence upon the interfiber distance. We indeed recover the observation made with the average evaporation rate: there is a unique evaporation speed for drops, while columns evaporate faster with a decreasing interfiber distance d.

We now study the dynamics in detail, starting with drops. We plot the length of the drop (normalized by the initial length) with respect to time $(t_f - t)$. The results collapse toward a single curve but do not exhibit a clear scaling law (Figure 4a). The shape of the drop between the fibers is complex and cannot be found analytically. However, we make the assumption that the evaporation of the drop is similar to that

dx.doi.org/10.1021/la4011532 | Langmuir XXXX, XXX, XXX–XXX

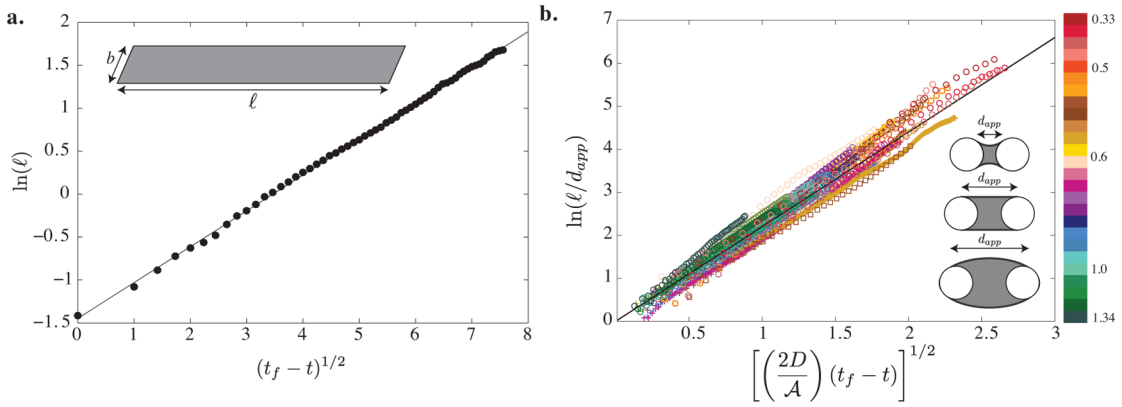

Figure 5. Evaporation of a column. (a) Evolution of $\ln(l)$ (in mm) with $(t_f - t)^{1/2}$ (in $s^{1/2}$) for $d/r = 1.07$ and SO65. Sketch of the equivalent strip of liquid used in the evaporation model. (b) Evaporation of columns for $2r = 0.2$ mm (○, +) and $2r = 0.35$ mm (□, ×) for silicone oils SO65 and SO1, respectively, and varying $0.33 < d/r < 1.34$.

of an aerosol droplet, only slightly affected by the fibers, as suggested by the universal behavior of the rescaled drop length, which is independent of the distance d/r. To verify this assumption, we measure the evolution of the mass of the evaporating drop with time (Figure 4b). The mass of the drop is typically small (2 mg). To measure fine variations of mass, we developed the setup sketched in the inset of Figure 4b. The fibers are attached to the coil of a sensitive displacement sensor, a rotary variable differential transformer (RVDT). As the mass decreases, the sensor rotates, which generates a current that can then be related to the drop mass after calibration. We can then measure the mass with an accuracy of 10^{-3} μg and, hence, deduce the drop volume V. We define an effective radius $R_{eff} = (3V/4\pi)^{1/3}$. The evolution of R_{eff} with time is given in Figure 4. The data for the two oils collapse onto a single curve, which is given exactly by the law

$$R_{eff} = (2D(t_f - t))^{1/2} \tag{2}$$

with the values of D found previously. The evaporation of the drop thus corresponds, to a first approximation, to the evaporation of an aerosol droplet of radius R_{eff} and is only slightly affected by the exact shape of the drop on the fibers.

We next focus on the columns that exhibit a strikingly different dynamics (Figure 3b). To understand the dynamics, we consider a thin rectangular wet strip of width b and length l such that $l \gg b$, as sketched in Figure 5a. We consider the solution of the steady-state diffusion equation outside the narrow strip, which is analogous to the electrostatic problem of a conducting ellipsoid with a large aspect ratio.[31] In this case, the diffusive flux occurs over distances approximately $b \ln(l/b) \gg b$, and therefore, the mass flux from the strip is about

$$j_0 = -\frac{D}{b \ln(l/b)} \tag{3}$$

The liquid volume is given by $V = l\mathcal{A}$, where $\mathcal{A}$ is the cross-sectional area of the column (inset in Figure 5b), while the exposed surface area is $A = lb$. The mass balance equation thus reads

$$\frac{\ln(l/b)}{l}\frac{dl}{dt} = -\frac{D}{\mathcal{A}} \tag{4}$$

which has the solution

$$\ln(l/b) = \left(\frac{2D}{\mathcal{A}}(t_f - t)\right)^{1/2} \tag{5}$$

We plot the evolution of $\ln(l)$ with $(t_f - t)^{1/2}$ in Figure 5a and observe excellent agreement with the experimental measurements for every experiment (i.e., varying d, r, or the liquid).

We now have to verify the pre-factor; we thus need to determine b and $\mathcal{A}$. We choose $b = d_{app}$ the distance wetted by the liquid (see inset in Figure 5b), which can be calculated analytically, together with $\mathcal{A}$ the cross-sectional area of the column.[25,27] We plot the rescaled data in Figure 5b. The data gather well onto a single line given by eq 5 with a prefactor of 2. We believe that the small scatter in the data and the missing prefactor are due to the assumption of the rectangular strip model, which does not consider the curvature of the interface and the liquid corners on the fibers (see inset in Figure 5b). A more refined model is thus needed to better quantify the dynamics, but our proposed model captures well the main trends in time and with variations in material and geometric parameters. We remark parenthetically that although droplets and columns have different surface curvatures, one can show that the Kelvin effect (the change in equilibrium vapor pressure above a curved surface) is negligible for this problem because the radius of curvature is always much larger than the molecular length scale.

FLEXIBLE FIBERS

On flexible fibers, the transition from drops to columns can be induced by the deformation of the fibers because of the capillary forces applied by the drop. We consider a pair of parallel flexible fibers of length L and bending stiffness B, clamped at one end with a fixed separation distance d and free to deflect at the other end. The liquid morphology is given by an elastocapillary balance that depends upon both the fiber properties and the volume of the drop.

We previously identified two critical volumes that determine the equilibrium state of a finite volume of liquid deposited on a pair of flexible fibers.[18] For $V > V_s$, the liquid adopts a compact drop shape. For $V < V_c$, the liquid adopts the shape of a long liquid column spread between coalesced fibers. For $V_s > V > V_c$, there is an intermediate state where the drop is only partially spread, with a small drop remaining at the edge. The critical volumes correspond to two elastocapillary balances

dx.doi.org/10.1021/la4011532 | Langmuir XXXX, XXX, XXX−XXX

$$V_s = \left(18\frac{\gamma d_s r L^3}{B(d - d_s)}\right)^3 \quad (6)$$

$$V_c = \pi r^2 (L - L_{ec}) \quad (7)$$

with

$$L_{ec} = \left(\frac{9Bd^2}{2\gamma r(\pi - 2)}\right)^{1/4} \quad (8)$$

where $d_s \simeq 1.1r$ is the average critical distance found experimentally at which the drop−column transition occurs and L_{ec} is an elastocapillary length, which represents the minimal distance along which the fibers can be bent by capillary forces. Hence, L_{ec} corresponds to the fiber length above which the deformation becomes significant. We thus expect to observe a strong dependence of the drying kinetics upon the fiber elasticity because of the changes in equilibrium morphology. Furthermore, the volume changes upon evaporation will lead to dynamical changes in morphology during drying.

Drying Kinetics. For a fixed volume V, as we increase the fiber length, we have a transition between drops on short, more rigid fibers ($L \leq L_{ec}$), to columns on long, more flexible fibers ($L > L_{ec}$). We measured the average evaporation rate ψ as a function of the ratio L/L_{ec} (Figure 6). We observe two regions:

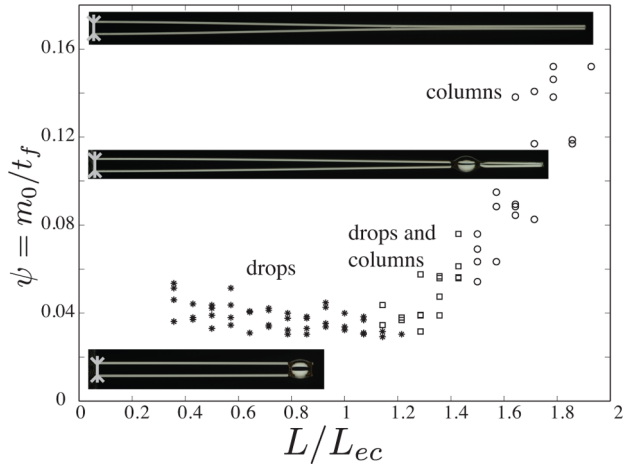

Figure 6. Average evaporation rate ψ (mg/s) on a pair of flexible fibers held on the left end at a distance d (arrows on the pictures) and free to move at the right end (glass fibers, $2r = 0.29$ mm, $B = 10^{-6}$ N m^2, and $d/r = 3.95$) as we increase the elasticity of the fibers (i.e., the ratio L/L_{ec}). We observe a transition from drops (stars) to columns (circles) with an intermediate region, where both states are observed (squares).

for rigid fibers, the liquid is in a drop state and the evaporation rate is constant, and for flexible fibers, the liquid is in the column state and the evaporation rate increases with an increasing deformation, i.e., with increasing flexibility (either decreasing fiber stiffness B, increasing length L, or decreasing distance d). There is an intermediate region where the liquid adopts both states during evaporation, which we will discuss in the next section. We thus recover the results obtained on rigid fibers. These results suggest that we can control the evaporation rate by controlling the deformation, i.e., the effective elasticity, of the fibers over a wide range (factor 4 change in the rate).

Morphology Transitions. As described earlier, large volumes of liquid ($V > V_s$) adopt a compact drop shape, while smaller volumes spread into either a partial ($V_s > V > V_c$) or total ($V < V_c$) liquid column. As the drop evaporates, we thus expect to observe morphology transitions, from drops to columns or from partial to total spreading. Here, the surface tension effect dominates, and changes in shape are fast enough to consider that the drop adopts successive equilibrium shapes as the volume decreases during evaporation. Examples of such dynamics are presented in Figure 7. We first consider the case where the initial volume V_0 is such that $V_s > V_0 > V_c$: the liquid first spreads into a column, with a small drop remaining at the edge (Figure 7a). As the liquid evaporates, the length of the column increases as the edge drop decreases in size. When the edge drop has disappeared, the liquid is in a total spreading morphology and the column has the maximum wet length $L - L_{ec}$. The column then decreases similarly to that between close rigid parallel fibers until complete evaporation.

A second transition is presented in Figure 7b for $V_0 > V_s$. We start with an hemi-spherical drop, whose size decreases with a decreasing volume. We note that the fibers become closer together, illustrating the increase of the capillary force applied by the drop as the volume is reduced. Then, suddenly, as $V = V_s$, the drop spreads into a column, after which the column length decreases. For more rigid fibers, the liquid remain as a drop for the total evaporation time. In addition, we can monitor the change of mass with time using the device presented in Figure 4, as shown in Figure 7c. For the partial/total column case, the mass decreases smoothly with time and there is no obvious transition. Similarly, for the drop case, the mass decreases smoothly in a similar fashion as in the rigid case. For the case where a drop−column transition occurs upon drying, we first observe the drop behavior followed by a sudden transition (indicated by an arrow) that is accompanied by a sharp acceleration of the drying rate, in agreement with our previous observations. These results show that liquid is redistributed as the drop evaporates and that wetting can be induced by drying. Measurement of the mass at the transition gives the spreading volume $V_s = 0.5$ μL, which is very close to the predicted value $V_s = 0.51$ μL calculated from eq 6. Furthermore, we can estimate the time at which this spreading transition occurs, which could be of practical significance. For a drop of initial volume V_0 and effective radius $R_0 = (3V/4\pi)^{1/3}$, the total evaporation time t_f is given by eq 2.

$$t_f = \frac{R_0^2}{2D} \quad (9)$$

The drop reaches a volume V_s (or an effective radius R_s) for $t = t_s$ defined as

$$t_s = t_f - \frac{R_s^2}{2D} \quad (10)$$

In the case presented in Figure 7c, $V_0 = 1.4$ μL, $V_s = 0.5$ μL, and we find $t_s = 376$ s, which gives a good estimate of the time obtained experimentally ($t_s = 332$ s).

CONCLUSION

When deposited on a fiber array, liquid is distributed either in the form of long liquid columns or semi-spherical compact droplets, depending upon the structure of the array (i.e., the distance between the fibers) and its elasticity. The two liquid morphologies show distinct dynamics of evaporation. Columns evaporate significantly faster than drops because of their increased surface area and geometry. We demonstrate that the diffusive flux from a thin liquid column is strongly dependent

dx.doi.org/10.1021/la4011532 | Langmuir XXXX, XXX, XXX−XXX

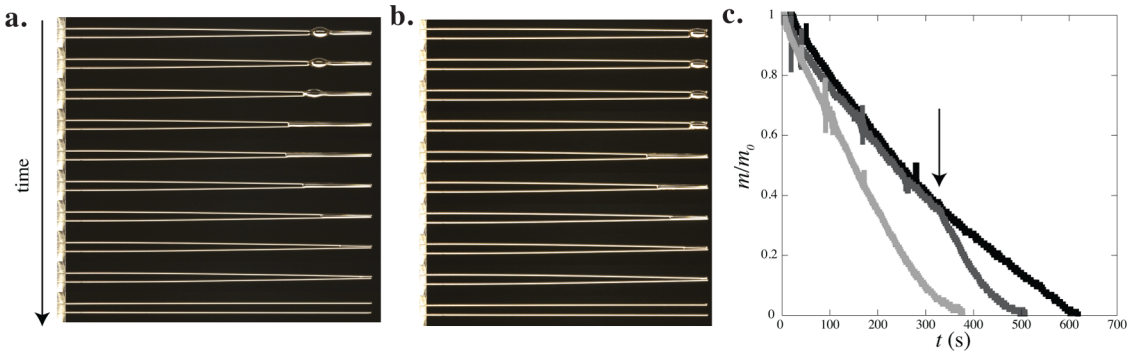

Figure 7. Time sequence of an evaporating drop of silicone oil SO65 of volume $V = 5\ \mu L$ on flexible glass fibers ($d/r = 3.8$ and $2r = 0.29$ mm) of lengths (a) 4.2 cm and (b) 3.6 cm. Interval between successive images = 10 s. (c) Evolution of the mass (in comparison to the initial mass $m_0 = m(t = 0)$) with time for a drop of volume 1.4 μL on glass fibers ($d/r = 4.2$ and $L_{ec} = 3$ cm), SO1, and different lengths exhibiting three regimes: a drop remains spherical (black, $L = 3$ cm), a drop transitions to a column (dark gray, $L = 3.7$ cm), and a transition from partial to total column (light gray, $L = 4.8$ cm).

upon the aspect ratio. Because the transition from drops to columns can be induced by the deformation of the fibers, a flexible material, in which fibers are allowed to bend, evaporates faster than a rigid material. It is thus possible to control the evaporation rate of the material indirectly by adjusting the fiber elasticity or deforming the matrix to change the liquid morphology. Furthermore, we have shown that, under particular conditions, the liquid can redistribute upon drying, i.e., spread into a long liquid column at a specific time during the evaporation process. We expect such rearrangements to have various consequences in fibrous media, such as the sudden collapse of adjacent fibers or the pattern obtained by deposition of solid particles during the evaporation of suspensions. Finally, the dynamics of evaporation of isolated droplets on a pair of fibers could provide new insights into the drying dynamics of more complex fibrous materials.

APPENDIX: DROP ON A SINGLE FIBER

We consider a drop sitting on a fiber of radius r, as sketched in Figure 8. The equilibrium contact angle is θ_e ($\theta_e = 0$ in the perfectly wetting case considered in this paper). Here, s measures arc length along the drop profile $z(x)$, and θ is the slope of the profile tangent, so that $dz/ds = \sin\theta$ and $dx/ds = \cos\theta$.

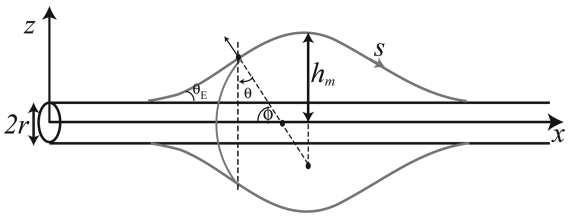

Figure 8. Shape of a drop sitting on one fiber.

To determine the profile, we need to solve the equation[30,32]

$$-\frac{d\theta}{ds} + \frac{\cos\theta}{z} = \frac{\Delta p}{\gamma} \tag{11}$$

where Δp is the capillary pressure. Using the boundary conditions at the apex of the drop ($\theta = 0$ at $z = h_m$) and at the contact line ($\theta = \theta_e$ at $z = r$), we obtain an expression for the capillary pressure and eq 11 becomes

$$z\cos\theta = \frac{z^2 + arh_m}{ar + h_m} \tag{12}$$

where

$$a = \frac{h_m\cos\theta_e - r}{h_m - r\cos\theta_e} \tag{13}$$

as introduced by Carroll.[30] We note that $a = 1$ in total wetting. Knowing that $\cos\theta = dx/ds = (1 + (dz/dx)^2)^{-1/2}$, we solve eq 12 for the profile

$$x(z) = \int_z^{h_m} \frac{z^2 + arh_m}{\sqrt{z^2 - a^2r^2}\sqrt{h_m^2 - z^2}}dz \tag{14}$$

This equation can be further reduced to a form involving elliptic integrals by changing variables to ϕ defined as

$$z^2 = h_m^2(1 - k^2\sin^2\phi) \tag{15}$$

where

$$k^2 = 1 - \frac{a^2r^2}{h_m^2} \tag{16}$$

We finally obtain the profile

$$x(z) = h_mE(\phi, k) + arF(\phi, k) \tag{17}$$

where $F(\phi,k)$ and $E(\phi,k)$ are the incomplete elliptic integrals of the first and second kind, respectively. From there and for total wetting ($a = 1$), we deduce the wetted length on the fiber

$$l = 2[h_mE(k) + rK(k)] \tag{18}$$

where $K(k)$ and $E(k)$ are the complete elliptic integrals of the first and second kind, respectively. We can further obtain the surface area

$$A = 4\pi h_m(r + h_m)E(k) \tag{19}$$

and the volume

$$V = \frac{2\pi h_m}{3}[(2h_m^2 + 3h_mr + 2r^2)E(k) - r^2K(k)] - \pi r^2l \tag{20}$$

The mass balance (eq 1) thus reads

dx.doi.org/10.1021/la4011532 | Langmuir XXXX, XXX, XXX−XXX

$$\frac{dh_m}{dt} = -\frac{2DA}{l(dV/dh_m)} \quad (21)$$

where l, A, and V are given by eqs 18, 19, and 20, respectively. The equation is then solved numerically with MATLAB to obtain the evolution of the length $l(t)$.

AUTHOR INFORMATION

Corresponding Author

*E-mail: hastone@princeton.edu.

Present Address

‡Camille Duprat: PMMH, UMR 7636 du CNRS, ESPCI, 10 rue Vauquelin, 75005 Paris, France.

Notes

The authors declare no competing financial interest.

ACKNOWLEDGMENTS

We thank Unilever Research and the National Science Foundation (CBET-1132835) for support of this research.

REFERENCES

(1) Langmuir, I. The evaporation of small spheres. *Phys. Rev.* **1918**, *12*, 368−370.

(2) Cazabat, A.-M.; Guéna, G. Evaporation of macroscopic sessile droplets. *Soft Matter* **2010**, *6*, 2591.

(3) Erbil, H. Y. Evaporation of pure liquid sessile and spherical suspended drops: A review. *Adv. Colloid Interface Sci.* **2012**, *170*, 67−86.

(4) Bourgès-Monnier, C.; Shanahan, M. E. R. Influence of evaporation on contact angle. *Langmuir* **1995**, *14*, 2820−2829.

(5) Rowan, S. M.; Newton, M. I.; McHale, G. Evaporation of microdroplets and the wetting of solid surfaces. *J. Phys. Chem.* **1995**, *99*, 13268−13271.

(6) McHale, G.; Aqil, S.; Shirtcliffe, N. J.; Newton, M. I.; Erbil, H. Y. Analysis of droplet evaporation on a superhydrophobic surface. *Langmuir* **2005**, *21*, 11053−11060.

(7) Tsai, P.; Lammertink, R. G. H.; Wessling, M.; Lohse, D. Evaporation-triggered wetting transition forwater droplets upon hydrophobic microstructures. *Phys. Rev. Lett.* **2010**, *104*, 116102.

(8) Lester, G. R. Contact angles of liquids at deformable solid surfaces. *J. Colloid Sci.* **1961**, *16*, 315−326.

(9) Fortes, M. A. Deformation of solid surfaces due to capillary forces. *J. Colloid Interface Sci.* **1984**, *100*, 17−26.

(10) Pericet-Camara, R.; Best, A.; Butt, H.-J.; Bonaccurso, E. Effect of capillary pressure and surface tension on the deformation of elastic surfaces by sessile liquid microdrops: An experimental investigation. *Langmuir* **2008**, *24*, 10565−10568.

(11) Jerison, E. R.; Xu, Y.; Wilen, L. A.; Dufresne, E. R. Deformation of an elastic substrate by a three-phase contact line. *Phys. Rev. Lett.* **2011**, *106*, 186103.

(12) Style, R. W.; Dufresne, E. R. Static wetting on deformable substrates, from liquids to soft solids. *Soft Matter* **2012**, *8*, 7177−7184.

(13) Lopes, M. C.; Bonaccurso, E. Evaporation control of sessile water drops by soft viscoelastic surfaces. *Soft Matter* **2012**, *8*, 3875−3881.

(14) Pu, G.; Severtson, S. J. Water evaporation on highly viscoelastic polymer surfaces. *Langmuir* **2012**, *28*, 10007−10014.

(15) Kajiya, T.; Daerr, A.; Narita, T.; Royon, L.; Lequeux, F.; Limat, L. Advancing liquid contact line on visco-elastic gel substrates: Stick-slip vs. continuous motions. *Soft Matter* **2013**, *9*, 454−461.

(16) Sutter, B.; Bémer, D.; Appert-Collin, J.-C.; Thomas, D.; Midoux, N. Evaporation of liquid semi-volatile aerosols collected on fibrous filters. *Aerosol Sci. Technol.* **2010**, *44*, 395−404.

(17) Py, C.; Bastien, R.; Bico, J.; Roman, B.; Boudaoud, A. 3D aggregation of wet fibers. *EPL* **2007**, *77*, 44005.

(18) Duprat, C.; Protière, S.; Beebe, A. Y.; Stone, H. A. Wetting of flexible fibre arrays. *Nature* **2012**, *482*, 510−513.

(19) Kamo, J.; Hiram, T.; Kamada, K. Solvent-induced morphological change of microporous hollow fiber membranes. *J. Membr. Sci.* **1992**, *70*, 217−224.

(20) Pokroy, B.; Kang, S. H.; Mahadevan, L.; Aizenberg, J. Self-organization of a mesoscale bristle into ordered, hierarchical helical assemblies. *Science* **2009**, *323*, 237−40.

(21) Chandra, D.; Yang, S. Stability of high-aspect-ratio micropillar arrays against adhesive and capillary forces. *Acc. Chem. Res.* **2010**, *43*, 1080−1091.

(22) De Volder, M.; Tawfick, S. H.; Park, S. J.; Copic, D.; Zhao, Z.; Lu, W.; Hart, A. J. Diverse 3D microarchitectures made by capillary forming of carbon nanotubes. *Adv. Mater.* **2010**, *22*, 4384−4389.

(23) Minor, F. W.; Schwartz, A. M.; Wulkow, E. A.; Buckles, L. C. Part III: The behavior of liquids on single textile fibers. *Text. Res. J.* **1959**, *29*, 940−949.

(24) Miller, B.; Coe, A. B.; Ramachandran, P. N. Liquid rise between filaments in a V-configuration. *Text. Res. J.* **1967**, *37*, 919−924.

(25) Princen, H. Capillary phenomena in assemblies of parallel cylinders III. Liquid columns between horizontal parallel cylinders. *J. Colloid Interface Sci.* **1970**, *34*, 171−184.

(26) Keis, K.; Kornev, K. G.; Kamath, Y. K.; Neimark, A. V. *Nanoengineered Nanofibrous Materials*; Kluwer Academic Publishers: Dordrecht, The Netherlands, 2004; pp 173−180.

(27) Protière, S.; Duprat, C.; Stone, H. A. Wetting on two parallel fibers: Drop to column transitions. *Soft Matter* **2013**, *9*, 271−276.

(28) McHale, G. Global geometry and the equilibrium shapes of liquid drops on fibers. *Colloids Surf., A* **2002**, *206*, 79−86.

(29) Eral, H. B.; de Ruiter, J.; de Ruiter, R.; Oh, J. M.; Semprebon, C.; Brinkmann, M.; Mugele, F. Drops on functional fibers: From barrels to clamshells and back. *Soft Matter* **2011**, *7*, 5138.

(30) Carroll, B. The accurate measurement of contact angle, phase contact areas, drop volume, and Laplace excess pressure in drop-on-fiber systems. *J. Colloid Interface Sci.* **1976**, *57*, 488−495.

(31) Landau, L. D.; Lifšic, E. M.; Sykes, J. B.; Bell, J. S.; Kearsley, M.; Pitaevskii, L. P. *Electrodynamics of Continuous Media*; Pergamon Press: Oxford, U.K., 1960; Vol. *364*.

(32) Gennes, P.-G. D.; Brochard-Wyart, F.; Quere, D. *Gouttes, Bulles, Perles et Ondes*; Belin, Paris, France, 2005.